Received: 15 March 2022 | Accepted: 28 June 2022

DOI: 10.1002/hep4.2040

ORIGINAL ARTICLE

Co-regulation of hepatic steatosis by ferritinophagy and unsaturated fatty acid supply

Ning Li[1] | **Yilie Liao**[1] | **Haipeng Huang**[1] | **Suneng Fu**[2]

[1]School of Life Sciences, Tsinghua University, Beijing, China

[2]Department of Basic Research, Guangzhou Laboratory, Guangdong, China

Correspondence
Ning Li, School of Medicine, Tsinghua University, 30 Shuanqing Road, Haidian District, Beijing 100084, P.R. China.
Email: lining201391@163.com

Suneng Fu, Department of Basic Research, Guangzhou Laboratory, Guangzhou 510005, P.R. China.
Email: fu_suneng@gzlab.ac.cn

Funding information
National Key Research and Development Program of China, Grant/Award Number: 2016YFA0502002 and 2017YFA0504603; National Natural Science Foundation of China, Grant/Award Number: 31671229 and 81471072; Tsinghua-Peking Center for Life Sciences; Guangzhou Laboratory

Abstract

Both iron overload and iron deficiency have been reported in obesity and metabolic syndromes. Due to the presence of multiple intracellular iron pools and the dynamic nature of iron mobilization and use, the actual status and contribution of free and metabolically active iron toward metabolic syndrome remain to be established. The discovery of nuclear receptor coactivator 4 (NCOA4) as a ferritinophagy receptor provides an opening to address the connection between iron and metabolic diseases. This study aims to specifically dissect the role of hepatic ferritinophagy in lipid metabolism and hepatic steatosis. We conducted a series of *Ncoa4* gain- and loss-of-function experiments to examine how ferritinophagy affects lipid metabolism through phenotypic and lipidomic analyses both *in vitro* and *in vivo*. We show that ferritinophagy is required to release iron from ferritin cages for biological use, and is induced by lipid loading *in vitro* and during the development of obesity *in vivo*. *Ncoa4* knockdown impairs mitochondrial morphology and reduces palmitate-induced lipid droplet formation in cultured cells and the development of hepatic steatosis in obese mice models. Importantly, the effect of *Ncoa4* deficiency on mitochondrial morphology and lipid accumulation is specifically linked to lipidomic reductions in unsaturated fatty acid content in triglycerides and cardiolipins, and an external supply of unsaturated fatty acids reverses these phenotypes. *Conclusion*: This study shows that ferritinophagy-derived iron supports fatty acid desaturation and the synthesis of unsaturated fatty acid–rich lipids to reduce lipotoxicity. However, the continuous activation of ferritinophagy contributes to the development of hepatic steatosis and liver damage in obesity.

INTRODUCTION

Iron plays an essential role in many cellular processes as a prosthetic factor, including oxygen transport, mitochondrial respiration, fatty acid desaturation, and DNA biosynthesis.[1,2] However, the oxidative potential of free iron not bound to proteins is also highly detrimental through Fenton reaction and the formation of reactive oxygen species.[3] Therefore, iron homeostasis is carefully managed in the body.[1,4]

Perturbation in iron homeostasis is often observed in patients with obesity, insulin resistance, or nonalcoholic fatty liver disease (NAFLD), collectively referred to as the dysmetabolic iron overload syndrome (DIOS).[5,6] Oxidative stress is one of the primary mechanisms linking iron overload with NAFLD.[7] Not only does oxidative stress increase steatosis by causing apolipoprotein B100 degradation and impairing very-low density lipoprotein secretion,[8,9] but it also can aggravate steatosis by activating inflammatory pathways and cell death.[7,10,11]. Iron overloading may also directly activate AKT signaling, up-regulate fatty acid and cholesterol synthesis, cause endoplasmic reticulum stress, and activate hepatic macrophage and stellate cells. As a result, iron overload may accentuate liver damage and promote the development of hepatic steatosis toward nonalcoholic steatohepatitis (NASH).[11–14]

However, iron overload in obese patients and patients with NAFLD is modest and often falls within the high end of the normal range.[6,15] Therefore, it is unclear whether this modest iron overload may have a direct, causal role in aggravating hepatic steatosis *in vivo*. Moreover, the assessment of iron status *in vivo* varies depending on the kind of marker used. For example, transferrin saturation decreases as body mass index increases, indicative of a state of iron deficiency,[16,17] and it may be caused by the increased blood volume in obese/overweight individuals.[18,19] In contrast, the serum hepcidin concentration, an indicator of systemic iron overload, is elevated in the obese populations.[20,21] Discrepancies among iron-reported gene levels suggest the involvement of additional factors (e.g., inflammation) in regulating their expression.[20,22,23] Thus, the actual status of free and metabolically available iron in obese and NAFLD animal models and patients warrants further study.[24]

Most of the intracellular iron pool is stored in ferritin cages and is released in the lysosome following intracellular iron starvation, to support the synthesis of heme and iron–sulfur clusters.[25–27] Nuclear receptor coactivator 4 (NCOA4) is the cargo receptor mediating autophagic turnover of ferritin (i.e., ferritinophagy).[28,29] Cell and animal models of NCOA4 deficiency confirm iron mobilization through ferritinophagy being essential for mitochondrial function, erythropoiesis, and even cell death.[30–33] Moreover, NCOA4-driven ferritinophagy responds to intracellular iron availability to promote iron homeostasis; specifically, the ubiquitin E3 ligase HERC2 (HECT and RLD domain containing E3 ubiquitin protein ligase 2) binds to NCOA4 in an iron-dependent manner to drive its proteasomal degradation and fine-tune iron mobilization.[31]

Here we report the identification of a ferritinophagy–fatty acid desaturation axis that governs iron and lipid homeostasis.

EXPERIMENTAL PROCEDURES

Animal studies

All animal protocols were approved by the Institutional Animal Care and Use Committee of Tsinghua University (Beijing, China). All mice were maintained on a 12-h/12-h light/dark cycle in a pathogen-free barrier facility at Tsinghua Laboratory Animal Research Center at controlled temperature (23 ± 2°C) with free access to water and food. Male mice aged 8–12 weeks (except the high-fat diet–fed mice) were used in respective experiments.

The *Ncoa4*$^{fl/fl}$ mouse model was generated by Cyagen with LoxP sites flanking the exon 2–6 of the mouse *Ncoa4* gene. Hepatocyte-specific *Ncoa4* knockout (KO) mice were generated by crossing *Ncoa4*$^{fl/fl}$ mice with Albumin-Cre transgenic mice (B6.Cg-Tg[Alb-Cre]21Mgn/J; The Jackson Laboratory). For the high-fat diet (HFD)–induced fatty liver mouse model, 4-week-old wild-type (WT) C57BL/6J mice were purchased from the Vital River Laboratory Animal Technology Co. and placed on HFD (D12492; 60 kcal% fat; Research Diets) for 16 weeks. Male leptin-deficient (*ob/ob*) mice were purchased from Hua Fukang Biotechnology Co. All the virus administrations *in vivo* were carried out by tail-vein injection. *Ncoa4* knockdown in mice was generated by adenovirus-driven expression of targeting short hairpin RNA. HFD and *ob/ob* mice with *Ncoa4* knockdown were sacrificed after 6 h of food withdrawal (9:00 a.m.–3:00 p.m.) 10 days following virus administration. Liver-specific green fluorescent protein (GFP) and NCOA4-FLAG overexpression in WT mice were achieved by an intravenous injection of adeno-associated virus (AAV 2/8; 1×10^{11} genome copies per mouse).

Primary hepatocytes isolation and culture

Primary hepatocytes were isolated from 8–10-week-old male mice. Briefly, mice were anesthetized with 250 mg/kg avertin, and the liver was perfused through the portal vein with 50 ml of prewarm Hank's balanced salt solution (HBSS) buffer (37°C) containing 0.25 mm ethylene glycol tetraacetic acid at a speed of 11 ml/min. The liver was then digested with 5–10 mg Collagenase IV (C5138; Sigma) prepared in an HBSS buffer supplemented with 5 mm $CaCl_2$. The liver was then excised, minced, and filtered through a 100-μm steel mesh. After washing twice with Medium 199 (MACGENE), primary hepatocytes were seeded into 0.1% gelatin-coated and air-dried 12-well plates at a density of 2×10^5 cells/well in BFM199 medium (0.2% bovine serum albumin [BSA], 2% fetal bovine serum [FBS], and 1% penicillin/streptomycin) for 4 h at 37°C with 5% CO_2. The culture was then washed and replaced with

fresh Medium 199 supplemented with 1 mg/ml Primocin (ant-pm-2; InvivoGen) and then cultured for designated analyses.

Cell lines

HepG2 and HEK293FT cells were obtained from ATCC. HEK293A was purchased from Thermo Fisher Scientific. Cells were cultured in Dulbecco's modified Eagle's medium containing 10% FBS at 37°C in a 5% CO_2 humidified atmosphere.

Statistical analysis

Data are presented as mean ± SEM. Statistical significance was evaluated by unpaired Student's *t* test or one-way analysis of variance followed by Bonferroni or Tukey *post hoc* test. A value of $p < 0.05$ was regarded as statistically significant.

Additional methods

Details of additional assays are described in the Supporting Information.

RESULTS

Hepatic ferritinophagy ensures physiological iron sufficiency

Apart from being the primary site for storage of excess body iron in ferritin cages, the liver has a high metabolic requirement for iron as a prosthetic factor.[34] The identification of NCOA4 as the receptor for lysosomal ferritin degradation[29] made it possible to examine how iron mobilization rather than deposit in ferritin cages may regulate metabolism and affect the pathogenesis of the metabolic syndrome.

We first created a hepatocyte-specific *Ncoa4* deletion model (*Ncoa4*^{HepKO}) to assess the role of ferritinophagy on local and systemic iron homeostasis (Figure 1A). Hepatocyte *Ncoa4* deletion resulted in near-complete ablation of *Ncoa4* transcript and protein expression in the liver, but not in other tissues (Figure 1A and Figure S1A). In the absence of NCOA4-mediated lysosomal degradation, ferritin accumulated in *Ncoa4*^{HepKO} liver tissues (Figure 1A). Hepatic non-heme iron is primarily stored in ferritin cages, and it increased in the KO liver as the result of a blunted ferritinophagy (Figure 1B). Perl's Prussian blue staining also confirmed higher iron retention in *Ncoa4*^{HepKO} liver (Figure S1B). Therefore, ferritinophagy is actively engaged in the turnover of ferritin and ferritin-stored irons under normal physiological conditions.

The lack of ferritinophagy-derived iron was sensed by the hepatic iron homeostasis system. Hepcidin (*Hamp1*) is a hepatic hormone that inhibits the export of iron from the duodenum and spleen into the circulatory system under hepatic iron overload conditions. Its expression was downregulated in the *Ncoa4*-deleted liver (Figure 1C). The liver also secretes transferrin into the circulation to transport iron from the periphery back to the liver. Circulating transferrin level measured as plasma iron-binding capacity increased in the *Ncoa4*^{HepKO} mice (Figure 1D).

The coordinated suppression of hepcidin expression and increase in circulatory iron transport masked the physiological importance of hepatic ferritinophagy. Transcriptome analysis revealed limited changes in the expression of iron-binding and heme-binding genes (Figure 1E,F and Figure S1J). Moreover, the *Ncoa4*^{HepKO} mice showed no gross defect in overall birth rate, body weight, plasma glucose levels, lipid profiles, spleen iron content, serum ferritin levels, and blood count (Figure S1C–I).

We then opted for an acute *Ncoa4* liver-specific KD mouse model to study the functional role of hepatic

FIGURE 1 Hepatic ferritinophagy ensures physiological iron sufficiency. (A) Schematic illustration of the generation of hepatocyte-specific *Ncoa4* knockout (HepKO) mice, real time-polymerase chain reaction (PCR) measurements of hepatic nuclear receptor coactivator 4 (*Ncoa4*) transcript levels, and immunoblot measurements of hepatic NCOA4 and ferritin heavy chain 1 (FTH1) protein levels in 10-week-old *Ncoa4*$^{fl/fl}$ and *Ncoa4*-HepKO mice fed a normal chow diet (n = 6–7 mice/group). (B,C) Measurement of liver non-heme iron levels (B), and real time PCR measurement of hepatic Hepcidin (*Hamp1*) transcript levels (C) in 10-week-old *Ncoa4*$^{fl/fl}$ and HepKO mice fed a normal chow diet (n = 6–7 mice/group). (D) Measurements of serum total iron-binding capacity (TIBC) and serum iron (SI), and the calculated levels of unsaturated iron-binding capacity (UIBC, TIBC-SI) and transferrin saturation (Tf.Sat, SI/TIBC) in 10-week-old *Ncoa4*$^{fl/fl}$ and HepKO mice fed a normal chow diet (n = 7 mice/group). (E) Volcano diagram display of liver differential expression genes (DEGs) between *Ncoa4* HepKO and *Ncoa4*$^{fl/fl}$ mice (n = 4 mice/group). (F) Gene-set enrichment analysis (GSEA) enrichment score curve of genes involved in heme and ferrous iron binding in *Ncoa4* HepKO mice. Benjamini and Hochberg (BH)–corrected *p*-values are labeled on the bottom (n = 4 mice/group). (G–L) Schematic illustration of liver-specific knockdown of *Ncoa4* in C57BL/6J wild-type (WT) mice, measurements of hepatic *Ncoa4* transcript levels, and hepatic NCOA4 and FTH1 protein levels (G); liver non-heme iron levels (H); hepatic *Hamp1* transcript levels (I); serum TIBC, UIBC, SI, and Tf.sat (J); volcano diagram display of liver DEGs (K); and GSEA enrichment analysis of heme and ferrous iron binding (L) in *shLacZ* and *shNcoa4* mice (n = 4–8 mice/group). (M–P) Schematic illustration of liver-specific overexpression of *Ncoa4* in C57BL/6J WT mice, measurements of hepatic *Ncoa4* transcript levels, and hepatic NCOA4 and FTH1 protein levels (M); liver non-heme iron levels (N); hepatic *Hamp1* transcript levels (O); serum TIBC, UIBC, SI, and Tf.sat (P) in WT mice expressing adeno-associated virus 8 (AAV8)–green fluorescent protein (GFP) or Ncoa4-Flag (n = 6 mice/group). Data are presented as mean ± SEM; *$p < 0.05$, **$p < 0.01$, ***$p < 0.001$, ****$p < 0.0001$; Student's *t* test (see also Figure S1). mRNA, messenger RNA.

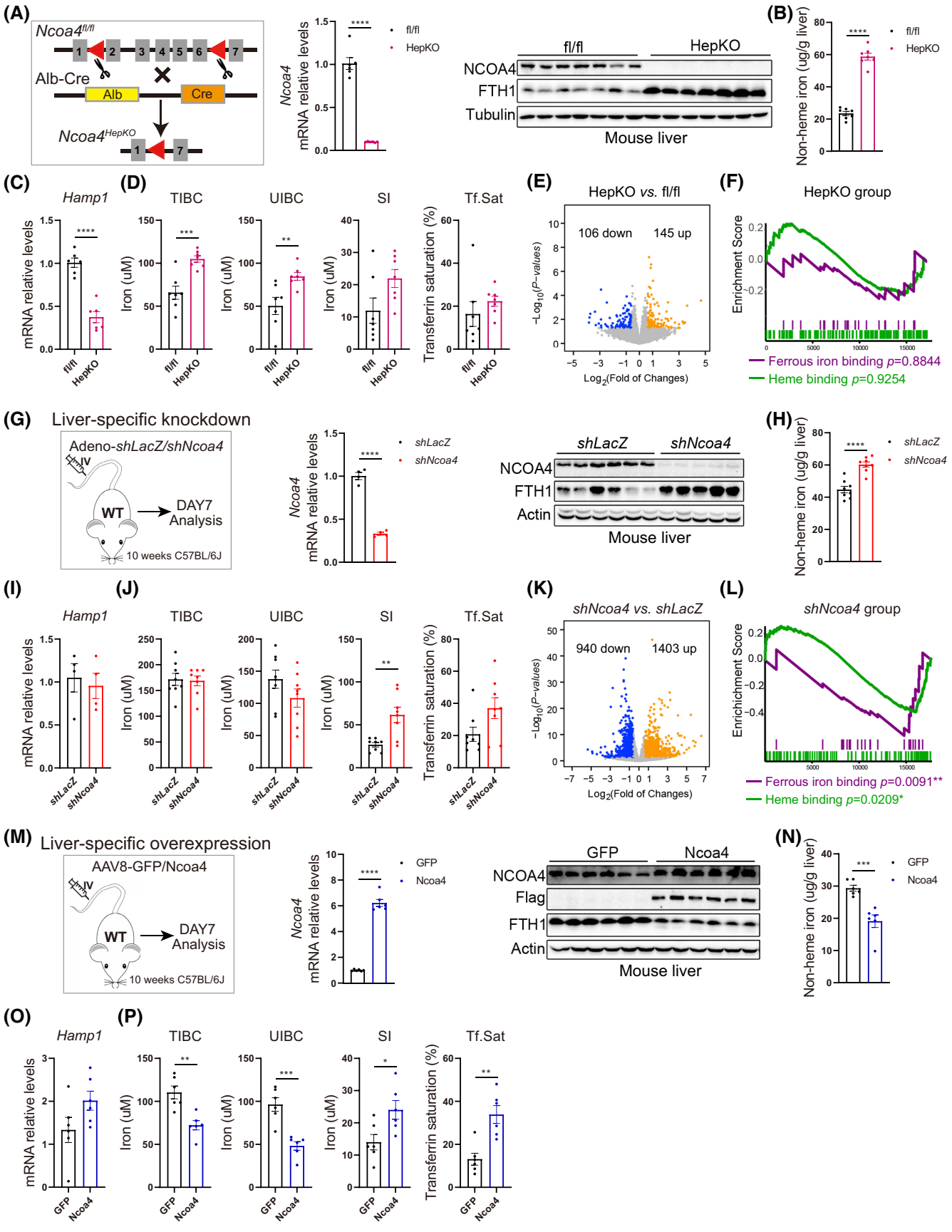
(A)
Ncoa4fl/fl
Alb-Cre
Alb
Cre
Ncoa4HepKO
Ncoa4 mRNA relative levels
fl/fl
HepKO
NCOA4
FTH1
Tubulin
Mouse liver
(B)
Non-heme iron (ug/g liver)
(C)
Hamp1
mRNA relative levels
(D)
TIBC
UIBC
SI
Tf.Sat
Iron (uM)
Transferrin saturation (%)
(E)
HepKO vs. fl/fl
106 down
145 up
−Log10(P-values)
Log2(Fold of Changes)
(F)
HepKO group
Enrichment Score
Ferrous iron binding p=0.8844
Heme binding p=0.9254
(G)
Liver-specific knockdown
Adeno-shLacZ/shNcoa4
IV
WT
DAY7
Analysis
10 weeks C57BL/6J
shLacZ
shNcoa4
Actin
(H)
(I)
(J)
(K)
shNcoa4 vs. shLacZ
940 down
1403 up
(L)
shNcoa4 group
Ferrous iron binding p=0.0091**
Heme binding p=0.0209*
(M)
Liver-specific overexpression
AAV8-GFP/Ncoa4
GFP
Ncoa4
Flag
(N)
(O)
(P)

ferritinophagy (Figure 1G,H and Figure S1K). In the *shNcoa4* mice liver, hepcidin gene expression was not down-regulated (Figure 1I), and serum iron-binding capacity did not increase (Figure 1J). There was also no significant difference in serum ferritin levels in control versus *shNcoa4* mice (Figure S1L). In the absence of a compensatory regulation in hepatic iron uptake, ferritinophagy deficiency caused a broad dysregulation of the transcriptome (Figure 1K). Gene ontology analysis showed that the most significant down-regulated functions in the *shNcoa4* liver included iron-binding and heme-binding, monooxygenase, and oxidoreductase activities (Figure 1L and Figure S1J), indicative of functional iron deficiency.

We further created a gain-of-function model through AAV-mediated expression of NCOA4 ($Ncoa4^{LOE}$) in mice liver (Figure 1M). In contrast to *Ncoa4* deficiency, NCOA4 overexpression reduced hepatic ferritin levels (Figure 1M), and hepatic iron content decreased by about one third (Figure 1N), although Perl's staining was too weak to show the decrease accordingly (Figure S1M). In response to increased iron release through ferritinophagy, hepcidin gene expression in the $Ncoa4^{LOE}$ liver trended toward an increase (Figure 1O), and plasma iron-binding capacity was reduced significantly (Figure 1P). The increase in transferrin saturation (Tf.Sat) might be attributed to high hepatic ferritinophagy and iron efflux (Figure 1P). Again, no obvious differences were observed for serum ferritin levels (Figure S1N).

Obesity up-regulates ferritinophagy to promote hepatic steatosis

After demonstrating the functional relevance of hepatic ferritinophagy in regulating iron homeostasis, we went on to ask how ferritinophagy and iron mobilization may be controlled and contribute to the development of obesity and hepatic steatosis.

Transcript measurements showed that the expression of *Ncoa4* was induced in the liver tissues of both the HFD-fed and genetically induced (*ob/ob*) obese mice (Figure 2A and Figure S2A). *Ncoa4* up-regulation was accompanied by increased NCOA4 protein levels and NCOA4– ferritin heavy chain 1 (FTH1) interaction (Figure 2A,B and Figure S2A,B). Notably, the amount of ferritin pulldown increased in obese samples despite lower levels of NCOA4 in the precipitate (Figure 2B and Figure S2B). Consequently, hepatic iron deposits decreased in the obese mice (Figure 2C and Figure S2C). Intriguingly, the increase in hepatic ferritinophagy in the obese liver did not cause the iron overload response observed in lean, $Ncoa4^{LOE}$ *mice*. Instead, *Hamp1* expression decreased (Figure 2D and Figure S2D).

We conducted *Ncoa4* knockdown experiments to understand the potential role of hepatic ferritinophagy up-regulation in obese mice (Figure 2E–G and Figure S2E–G). Adenovirus-mediated suppression of *Ncoa4* expression on transcript and protein levels resulted in hepatic ferritin and non-heme iron accumulation in both the HFD and *ob/ob* mice models (Figure 2F,H and Figure S2F,H). However, despite previously reported association between hepatic iron overload and hepatic steatosis, hepatic lipogenic enzyme levels were reduced in the iron-accumulated, obese mice liver (Figure 2F and Figure S2F). Histology analysis and triglyceride measurement showed that hepatic steatosis in the obese mice was improved (Figure 2I,J and Figure S2I,J), and the liver weight was reduced (Figure 2K and Figure S2K). Hyperglycemia and indicators of liver damage also improved (Figure 2L,M and Figure S2L,M).

Down-regulation in lipogenesis likely reduced hepatic steatosis in the *shNcoa4* obese mice liver. Inefficient fatty acid desaturation might also contribute to such a phenotype, because (1) triglyceride synthesis in mice usually requires two molecules of unsaturated fatty acid and one molecule of saturated fat, and (2) fatty acid desaturation by the stearate-CoA desaturase requires iron as a cofactor.[35,36] We performed lipidomic analysis for the *shNcoa4* obese mice liver to explore this hypothesis.

On the lipid class level, improvement of hepatic steatosis in the *shNcoa4* obese mice liver was accompanied with reductions in phosphatidylcholine (PC) content and increases in phosphatidylethanolamine (PE) content (Figure 2N), consistent with our previous observation that obesity increases the PC/PE ratio.[37] On the fatty acid level, its composition varied greatly across different lipid species (Figure 2O). For example, cardiolipin (CL) was consisted primarily of linoleic acid (C18:2), a polyunsaturated fatty acid. In contrast, over 40% of the fatty acids in phosphatidylcholine were saturated (Figure 2O).

We calculated the ratio of palmitate over oleate as an indicator of fatty acid saturation, and it increased across all three phospholipids (Figure 2P). The increase was most prominent in CL, possibly due to its low baseline fatty acid saturation (Figure 2O). Detailed analysis showed that all palmitate-containing cardiolipin species increased by more than 2-fold, whereas linoleate-only species decreased significantly (Figure 2Q).

Fatty acid desaturation mechanistically connects ferritinophagy to triglyceride storage

Work by the Schaffer group established that palmitate is preferentially incorporated into membrane phospholipids, and desaturation of palmitate by the stearate-CoA desaturase (SCD1) quantitatively promotes triglyceride synthesis.[38] Therefore, we reasoned that the improvement in hepatic steatosis and increase in palmitate content in the *shNcoa4* obese mice lipidome might

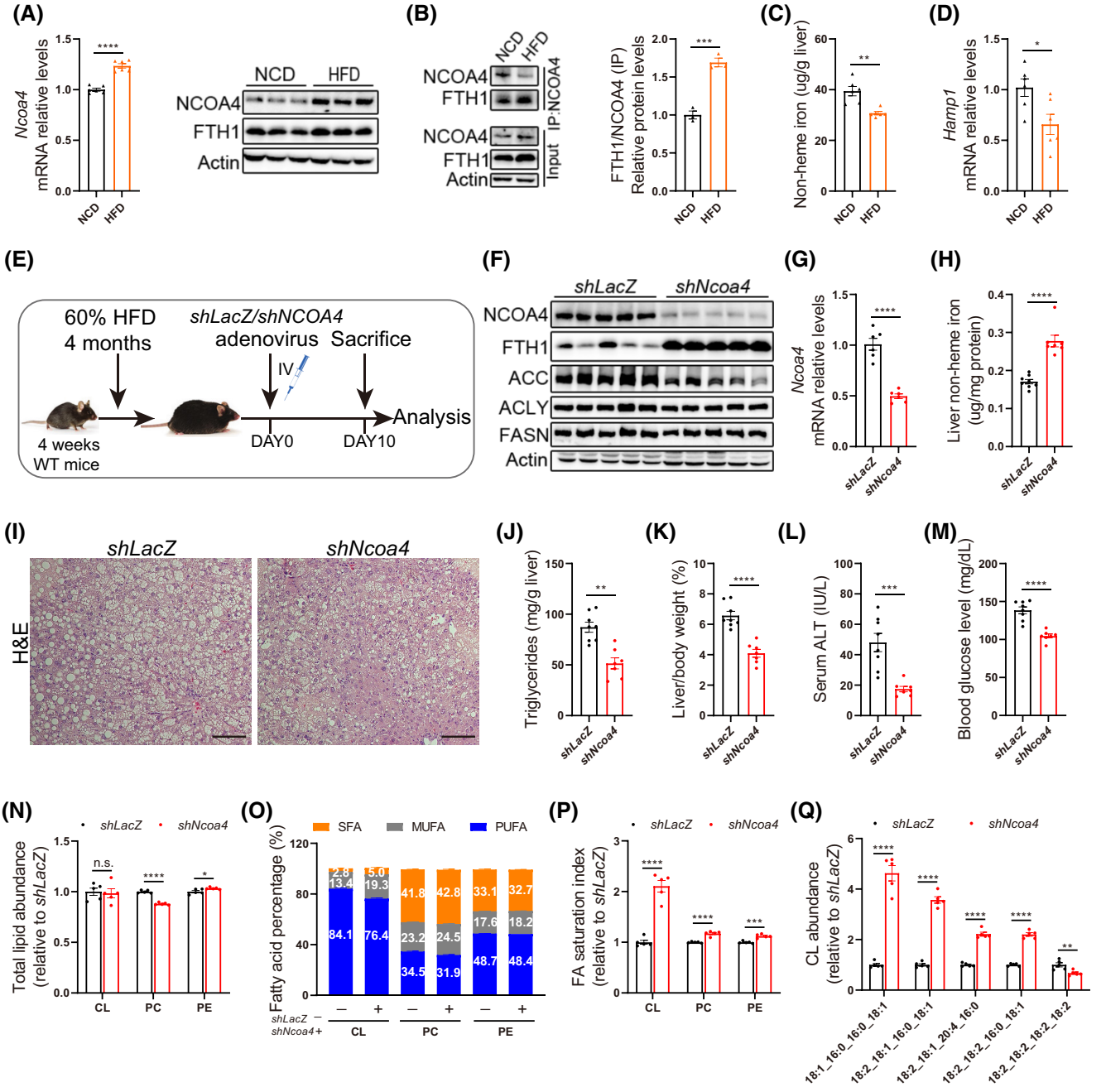

FIGURE 2 Ferritinophagy is induced in obese mice liver to promote triglyceride storage. (A–D) Real-time PCR measurements of *Ncoa4* transcript levels and immunoblot measurements of NCOA4 and FTH1 protein levels (A); co-immunoprecipitation (co-IP) measurements and quantification of NCOA4-FTH1 interactions (B); measurements of liver non-heme iron levels (C); and real-time PCR measurements of *Hamp1* transcript levels (D) in the liver lysates of high-fat diet (HFD; 4 months)–induced obese mice (n = 6 mice/group). Each lane of immunoblots in (A) and (B) are the mixture of two or six samples, respectively. (E) Schematic illustration of experimental design for *Ncoa4* knockdown in HFD mice. (F–H) Immunoblot analysis of NCOA4, FTH1, and *de novo* lipogenesis enzyme protein levels (F); quantitative PCR measurements of *Ncoa4* transcript levels (G); and quantification of the non-heme iron levels (H) in the liver tissues of *shLacZ* and *shNcoa4* HFD mice (n = 7–8 mice/group). (I–M) Hematoxylin and eosin (H&E) staining (I), liver triglyceride (TG) content (J), liver weight–to–body weight ratio (K), serum alanine aminotransferase (ALT) levels (L), and blood glucose levels (M) of *shLacZ* and *shNcoa4* HFD mice (n = 7–8 mice/group; scale bar, 100 μm). (N–Q) Mass spectrometry quantification of the relative abundance of total cardiolipin (CL), phosphatidylcholine (PC), and phosphatidylethanolamine (PE) levels (N); the fatty acid compositions of CL, PC, and PE (O); calculated indices of fatty acid saturation (C16:0/C18:1) for CL, PC, and PE (P); and the measured C16:0-containing or C18:2-only CLs (Q) in the liver tissues of *Ncoa4*-deficient HFD mice (n = 5 mice/group). Data are presented as mean ± SEM; *$p < 0.05$, **$p < 0.01$, ***$p < 0.001$, ****$p < 0.0001$; Student's *t* test (see also Figure S2). MUFA, monounsaturated fatty acid; NCD, normal-chow diet; n.s., not significant; PUFA, polyunsaturated fatty acid; SFA, saturated fatty acid.

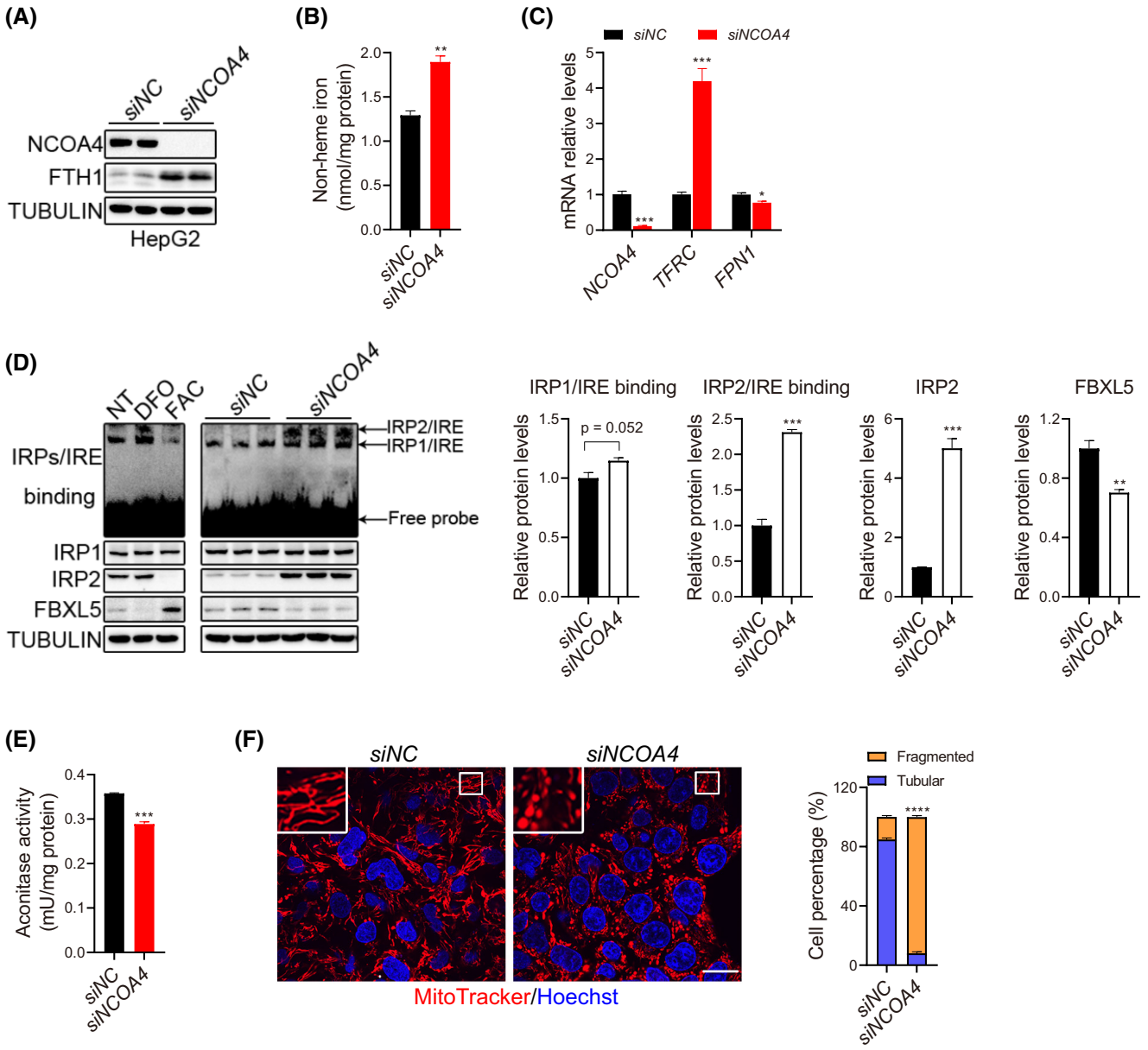

FIGURE 3 Knockdown of *NCOA4* in HepG2 hepatocytes results in iron starvation. (A) Immunoblot measurements of NCOA4 and FTH1 protein levels in HepG2 cells transfected with either scrambled small interfering RNA (siRNA) or *NCOA4* siRNA for 48 h. (B,C) Quantification of total non-heme iron level (B), and real time-PCR measurements of *NCOA4*, transferrin receptor (*TFRC*), and ferroportin 1 (*FPN1*) transcript levels (C) in *siNCOA4* (48 h) or control HepG2 cells. (D) Immunoblot measurements and quantification of iron-responsive element-binding protein (IRP)/iron-responsive element (IRE) binding, IRPs, F-box and leucine rich repeat protein 5 (FBXL5) protein levels in *siNCOA4* (48 h) or control HepG2 cells. HepG2 cells treated with deferoxamine mesylate (DFO; 100 μm) or ferric ammonium citrate (FAC; 25 μg/ml) for 24 h were lysed as the positive control. (E) Measurements of cellular aconitase activity in *siNCOA4* (48 h) or control HepG2 cells. (F) Confocal imaging of mitochondrial morphology in *siNCOA4* (48 h) or control HepG2 cells with MitoTracker Red (200 nm) staining. More than 100 cells were quantified for tubular or fragmented mitochondria. Scale bar, 20 μm. Data are presented as mean ± SEM; $*p < 0.05$, $**p < 0.01$, $***p < 0.001$, $****p < 0.0001$; Student's *t* test. NT, no treatment.

be attributed to defect in fatty acid desaturation. We used palmitate-induced and oleate-induced triglyceride synthesis system to elucidate the potential connection between ferritinophagy and fatty acid desaturation in hepatocyte cultures.

We first examined the engagement of ferritinophagy in cell culture. Similar to our observations in mouse liver, silencing the expression of the human *NCOA4* gene in HepG2 cells resulted in ferritin and iron accumulation *in vitro* (Figure 3A,B). Additionally, *NCOA4*-deficient HepG2 cells presented a series of iron-deficiency hallmarks that include the induction of transferrin receptor and the down-regulation of ferroportin 1 (Figure 3C), up-regulation of iron-responsive element-binding protein 2 and binding to iron-responsive element (Figure 3D), a reduction in the iron-sensitive E3-ubiquitin ligase

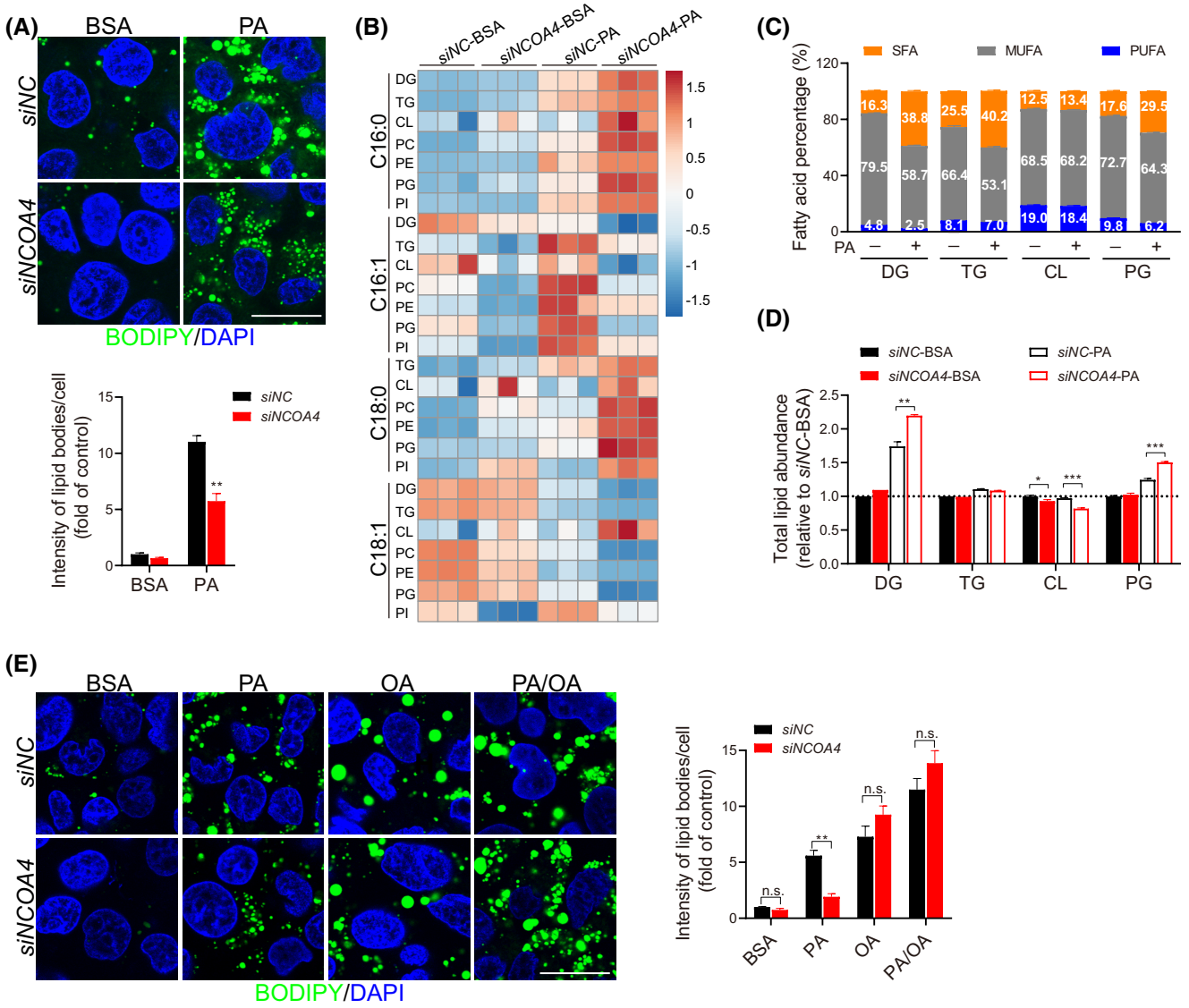

FIGURE 4 *NCOA4* deficiency impairs fatty acid desaturation and PA-induced triglyceride accumulation. (A) BODIPY 493/503 staining and quantification of lipid droplets in control or *siNCOA4* HepG2 cells. Cells were transfected with scrambled or *NCOA4* siRNA for 48 h, followed by 0.5 mm PA culture for 12 h. More than 100 cells were analyzed for the mean intensity of BODIPY signaling. Scale bar, 20 μm. (B) Heatmap display of perturbations of the fatty acid compositions of main lipid species in HepG2 cells treated as in (A). (C) Mass spectrometry quantification of the fatty acid compositions of diacylglycerol (DG), triglyceride (TG), CL, and phosphatidylglycerol (PG) in control (*siNC*) HepG2 cells cultured in the absence or presence of 0.5 mm PA for 12 h. (D) Mass spectrometry quantification of the relative abundance of DG, TG, CL, and PG in control and *siNCOA4* (48 h) HepG2 cells cultured in the absence or presence of 0.5 mm PA for 12 h. (E) BODIPY 493/503 staining and quantification of lipid droplets in control or *siNCOA4* HepG2 cells. Cells were transfected with either scrambled or *NCOA4* siRNA for 48 h, followed by palmitate (PA; 0.5 mm), oleate (OA; 0.5 mm), or PA/OA (0.5 mm/0.5 mm) challenge for 12 h. Scale bar, 20 μm. Data are presented as mean ± SEM; $*p < 0.05$, $**p < 0.01$, $***p < 0.001$; Student's *t* test (see also Figure S3). DAPI, 4′,6-diamidino-2-phenylindole; PI, phosphatidylinositol; TG, triglyceride.

FBXL5 (F-box and leucine rich repeat protein 5) protein levels (Figure 3D), and a decrease in aconitase activity (Figure 3E). The mitochondria also became fragmented and swollen (Figure 3F), another sign of iron deficiency in *siNCOA4* cells.

After confirming the presence and participation of ferritinophagy in regulating iron homeostasis *in vitro*, we examined how *NCOA4* deficiency might affect saturated fat (palmitate)–induced and unsaturated fat (oleate)–induced lipid droplet formation differently.

As shown in Figure 4A, culturing HepG2 cells with 0.5 mm of palmitate increased intracellular lipid droplet formation, and knockdown of *NCOA4* reduced lipid droplet formation by almost half (Figure 4A). The reduction in lipid droplet formation was not caused by reduced palmitate uptake based on the transcript and lipidomic analyses. The expression of fatty acid transporter clusters of differentiation 36 (CD36) and the lipidomic level of palmitate both increased in *siNCOA4* cells (Figure 4B and Figure S3A,B). Instead, palmitate

desaturation was specifically impaired in *siNCOA4* cells. As shown in Figure 4B and Figure S3B, the addition of palmitate (C16:0) to the medium caused a modest lipidomic increase in palmitate levels and a much larger increase in its desaturation product, palmitoleate, in the control cells (Figure 4B and Figure S3B). In contrast, the addition of palmitate to the *siNCOA4* cells caused a drastic increase in palmitate and its elongation product stearate, but not their desaturated product, palmitoleate and oleate (Figure 4B and Figure S3B). Consequently, the level of fatty acid saturation calculated by the ratio of (C16:0 + C18:0)/(C16:1 + C18:1) increased across all lipid species (Figure S3C,D).

The increase in fatty acid saturation was highest among diacylglycerides and phosphatidylglycerols (Figure S3D), lipid species that contain the highest levels of oleic acid (C18:1) (Figure S3B). As the HepG2 lipidome contains a limited amount of polyunsaturated fatty acid (Figure 4C), the limitation in oleate production shall limit the conversion of diacylglycerides to triglycerides and phosphatidylglycerol to cardiolipin. Consistent with this hypothesis, diacylglycerides and phosphatidylglycerols accumulated in *siNCOA4* cells (Figure 4D). At the same time, a significant decrease in cardiolipin content was detected (Figure 4D). However, the reduction in triglyceride content was not evident in mass spectrometry analysis (Figure 4D), possibly due to signal saturation.

Oleate culture experiments provided further support for such a hypothesis. As shown in Figure S3E, *siNCOA4* did not reduce oleate-induced lipid droplet formation in the HepG2 cells (Figure S3E). There was even a trend toward increased lipid droplet formation (Figure S3E), possibly attributable to CD36 up-regulation. Additionally, co-treatment of palmitate with oleate rescued the lipid droplet formation defect in the *siNCOA4* cells (Figure 4E). Therefore, *NCOA4* deficiency specifically reduces fatty acid desaturation and impairs saturated fatty acid–induced lipid droplet formation.

Saturated fatty acid stabilizes NCOA4 to activate ferritinophagy and reduce cell death

Triglyceride synthesis is a major protective mechanism in response to palmitate exposure.[38] Therefore, we asked whether cells specifically invoke ferritinophagy to protect them from palmitate toxicity through enhanced fatty acid desaturation and triglyceride synthesis.

Consistent with this view, palmitate, but not oleate, treatment of HepG2 cells induced the accumulation of the NCOA4 protein in a dose-dependent manner (Figure 5A). Importantly, NCOA4 protein accumulation in palmitate-treated cells was accompanied by a down-regulation of intracellular ferritin levels (Figure 5A), indicative of ferritinophagy activation. Furthermore, despite lower ferritin levels, considerably more ferritin was bound to NCOA4 in palmitate-treated cells than in control (Figure 5B).

Palmitate induced NCOA4 accumulation and ferritin-NCOA4 binding in primary hepatocytes to a similar degree to HepG2 cells (Figure 5C,D). However, no reduction of ferritin levels was observed in palmitate-treated primary hepatocytes (Figure 5C,D). The lack of lysosomal ferritin degradation in isolated primary hepatocytes allowed us to monitor palmitate-induced ferritinophagy by demonstrating ferritin recruitment to lysosomal compartments. To this end, we co-expressed the lysosome marker lysosomal-associated membrane protein 1 (LAMP1)–GFP with FTH1-mCherry in primary hepatocytes and examined their localization under normal and palmitate treatment conditions. As shown in Figure 5E, FTH1-mCherry fluorescence signals were normally dispersed intracellularly in the control cells, and it showed little overlap with the lysosome marker LAMP1-GFP. However, following the treatment of palmitate, FTH1-mCherry was co-localized with LAMP1-GFP in puncta (Figure 5E), supporting the induction of ferritinophagy.

Unlike obesity-induced NCOA4 expression *in vivo*, the elevation of NCOA4 protein levels in the

FIGURE 5 Palmitate activates ferritinophagy to reduce lipotoxicity. (A) Immunoblot measurements and quantification of NCOA4 and FTH protein levels in HepG2 cells treated with bovine serum albumin (BSA)–conjugated PA or OA for the indicated dose for 12 h. (B) Co-IP measurements and quantification of NCOA4-FTH1 interactions in HepG2 cells treated with PA for the indicated dose for 12 h. Control immunoglobulin G (IgG) immunoprecipitation (IP) lysate is the mixture of BSA and PA-treated samples. (C,D) Immunoblot measurements and quantification of NCOA4 and FTH protein levels (C) and co-IP measurements and quantification of NCOA4-FTH1 interactions (D) in mouse primary hepatocytes treated with PA for the indicated dose for 12 h. (E) Confocal imaging of the subcellular localization of exogenously expressed FTH1-mCherry and lysosomal-associated membrane protein 1 (LAMP1)–enhanced GFP (eGFP) in primary hepatocytes. Primary hepatocytes were infected with adenovirus-expressing mouse FTH1 and LAMP1 fusion proteins for 4 h, followed by treatment with 0.5 mm PA or BSA vehicle for 12 h. Scale bar, 5 μm. (F) Schematic illustration of experimental design for PA-induced lipotoxicity test in HepG2 cells. (G) Measurement of cell death by propidium iodide (PI) staining. HepG2 cells were transfected with either scrambled siRNA or *NCOA4* siRNA for 48 h, followed by 0.5 mm PA or BSA vehicle challenge for 12 h, and then cells were trypsinized, stained, and analyzed with flow cytometry. (H) Measurement of cell death by Hoechst 33342 staining. HepG2 cells were treated as in (G); cells deaths were shown by microscopy and results were quantified and normalized to *siNC*-BSA treatment (control). *Denotes statistical significance in comparison with control. Scale bar, 50 μm. (I) Measurement of cell death by detecting the level of lactate dehydrogenase (LDH) released into the culture medium. HepG2 cells were treated as in (G), and culture medium was collected for LDH analysis. Results were normalized to *siNC*-BSA treatment (control). *Denotes statistical significance in comparison with control. Data are presented as mean ± SEM; $^{*}p < 0.05$, $^{**}p < 0.01$, $^{***}p < 0.001$, $^{****}p < 0.0001$, $^{\#\#\#}p < 0.001$, $^{\#\#\#\#}p < 0.0001$, Student's *t* test (see also Figure S4).

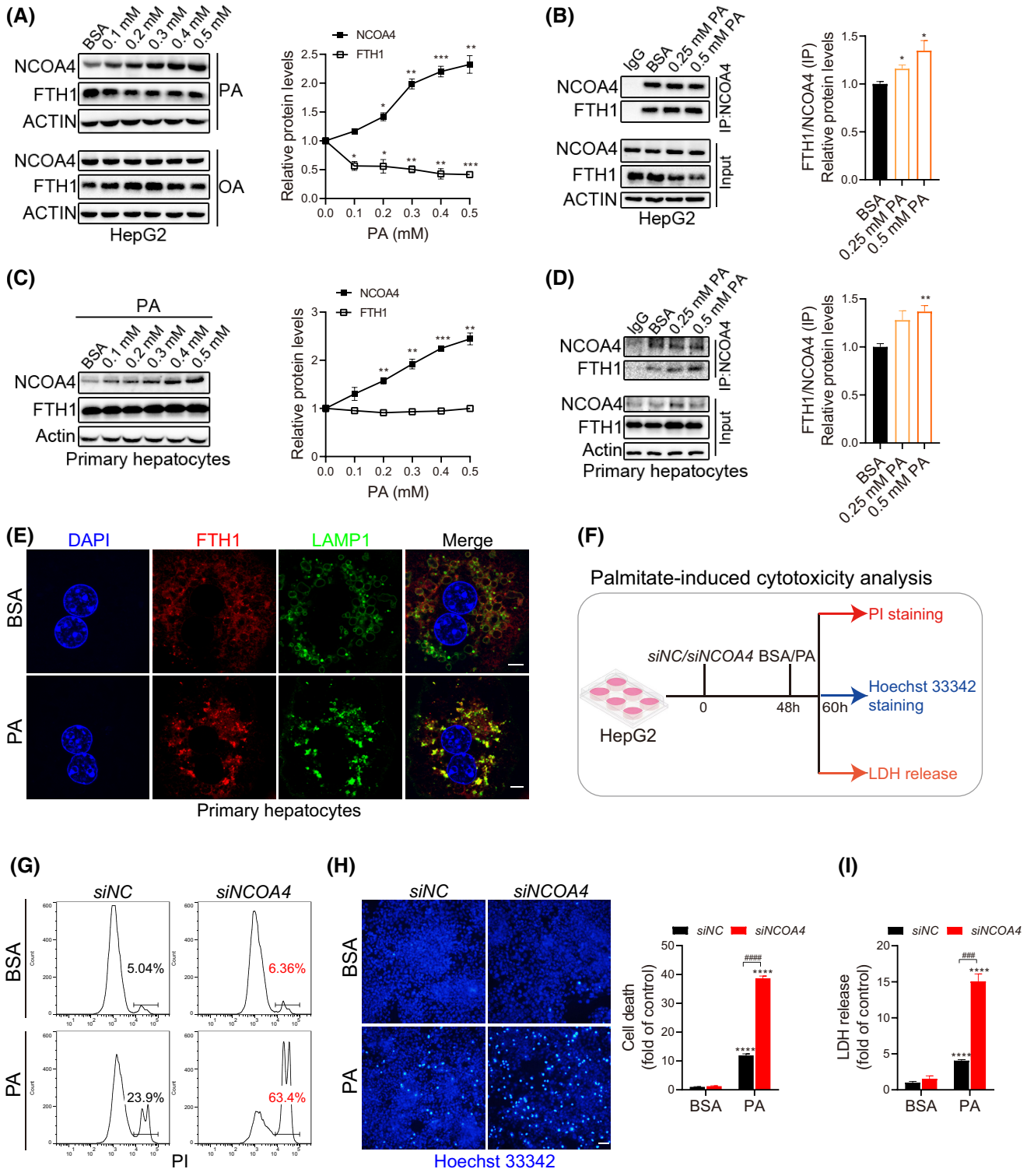

palmitate-treated HepG2 cells *in vitro* was not caused by transcriptional regulation (Figure S4A). Both NCOA4 and FTH1 were constitutively degraded through the lysosome and the proteasome, as treatment of cells with the proteasomal inhibitor MG132, the lysosome inhibitor chloroquine, and the autophagy inhibitor bafilomycin A1 all increased their protein levels (Figure S4B). Importantly, because co-treatment of HepG2 cells with MG132 and palmitate did not increase NCOA4 protein levels beyond palmitate treatment alone (Figure S4B), palmitate might stabilize NCOA4 protein through the proteasomal pathway. Proteasomal degradation of NCOA4 was mediated by the iron-dependent interaction between NCOA4 and the E3 ubiquitin ligase HERC2.[31] We measured intracellular labile iron pool by Calcein-AM and found about a 60% reduction in

palmitate-treated HepG2 cells compared with control cells (Figure S4C), consistent with a previous study.[39] Therefore, palmitate may activate ferritinophagy downstream of iron depletion.

We then applied both gain and loss-of-function approaches to finally examine the functional role of ferritinophagy on palmitate-induced toxicity (Figure 5F–I and Figure S4D–F). Measurement of cell death by propidium staining showed that *NCOA4* knockdown or overexpression did not affect cell viability under basal conditions (Figure 5G and Figure S4E). Palmitate treatment in the culture medium increased the percentage of apoptotic cells from about 4% to 24% (Figure 5G). NCOA4 overexpression reduced palmitate-induced cell death to 17.1% (Figure S4E), whereas *siNCOA4* more than doubled cell death to 63.4% (Figure 5G). Cell death measured by Hoechst 33342 staining and cytosolic lactate dehydrogenase release into the medium reached the same conclusion (Figure 5H,I and Figure S4F).

Fatty acid desaturation quantitively correlates with cell survival under palmitate treatment conditions.[38] As an additional confirmation, we carried out *SCD1* knockdown experiments and examined the effect of SCD1 deficiency on palmitate-induced cell death in a comparable system (Figure S4G). As shown in Figure S4H,I, *SCD1* deficiency led to a modest increase in cell death even under basal, BSA-treated cells, and palmitate-induced cell death reached about 60%, comparable to *siNCOA4* cells (Figure S4H,I). Therefore, ferritinophagy and desaturase play equivalent roles in protecting cells from saturated fatty acid–induced cell death.

Ferritinophagy is not required for re-esterification of fatty acids *in vivo*

Fasting up-regulates hepcidin expression, an indicator of iron overloading.[40] We found that *Ncoa4* was also up-regulated by fasting both on the transcript and protein levels (Figure S5A). Because the liver re-esterifies adipose tissue lipolysis–derived fatty acids under fasting conditions, we predicted that unsaturated fatty acid should not be limiting, and NCOA4 deficiency should not impair fasting-induced hepatic steatosis.

Indeed, hepatic steatosis was not ameliorated in the overnight-fasted *shNcoa4* lean mice compared with their *shLacZ* controls (Figure 6A–C and Figure S5B). Instead, more triglyceride accumulated in the *shNcoa4* liver and hepatocytes than in control (Figure 6C and Figure S5B), providing an *in vivo* support to our hypothesis that ferritinophagy-controlled triglyceride synthesis is dependent on fatty acid composition.

Despite increased triglyceride synthesis, *shNcoa4* lean mice hepatocytes presented swollen mitochondria (Figure 6D–F) and down-regulation in cardiolipin content (Figure 6G), similar to palmitate-treated *siNCOA4* HepG2 cells. The differential effect of NCOA4 deficiency on cardiolipin and triglyceride synthesis may be attributed to the fact that hepatic triglycerides were synthesized overnight from adipose triglyceride–derived fatty acids, while cardiolipin and other phospholipids were the product of the hepatic fatty acid pool over a long period. Fatty acid composition analyses provided support for this proposition.

As shown in Figure 6H, lean mice lipidome had more polyunsaturated fatty acids and less saturated fatty acids than their obese counterparts (Figure 6H). Knockdown of *Ncoa4* selectively increased fatty acid saturation in cardiolipins and phosphatidylcholines (Figure 6I,J), although to a less degree than *shNcoa4* obese mice liver and *siNCOA4* cells, but not in triglycerides (Figure 6I). Instead, fatty acid saturation in triglycerides was lower in *the shNcoa4* liver than in control (Figure 6I).

Mitochondrial dysfunction might increase hepatic steatosis observed in the *Ncoa4*-deficient liver. Additionally, transcript analysis found that the fatty acid transporter CD36 was also up-regulated in the *shNcoa4* liver tissues as in the *siNCOA4* HepG2 cells (Figure 6K and Figure S3A). Knockdown of *CD36* rescued the hepatic steatosis phenotype observed in overnight-fasted *shNcoa4* mice liver (Figure 6L,M and Figure S5C). Thus, ferritinophagy deficiency has the potential to increase triglyceride accumulation through CD36 induction.

DISCUSSION

Together, the results presented in this study indicate that ferritinophagy is essential for mobilizing iron from ferritin stores to support fatty acid oxidative desaturation and the synthesis of triglycerides and cardiolipins to reduce lipotoxicity. Although beneficial in the short term, the chronic induction of ferritinophagy likely contributes to the development of hepatic steatosis and severe liver disease in the long term.

Although the enzymatic requirement for iron in the proteome is well-established, our findings shed light into the seemingly non-deterministic relationship between iron and metabolic syndrome.[41,42] First, ferritinophagy activity may distort the relationship between iron accumulation and iron availability. As shown in our *Ncoa4* gain and loss-of-function studies, iron accumulation is inversely correlated with functional iron sufficiency (Figure 1B,C for *Ncoa4* knockout; Figure 1H,L for *Ncoa4* knockdown; Figure 1N,O for *Ncoa4* overexpression). Although the status of ferritinophagy in dysmetabolic iron overload syndrome (DIOS) has not been established, it is possible that iron accumulation may not quantitatively indicate functional iron sufficiency and overload. Second,

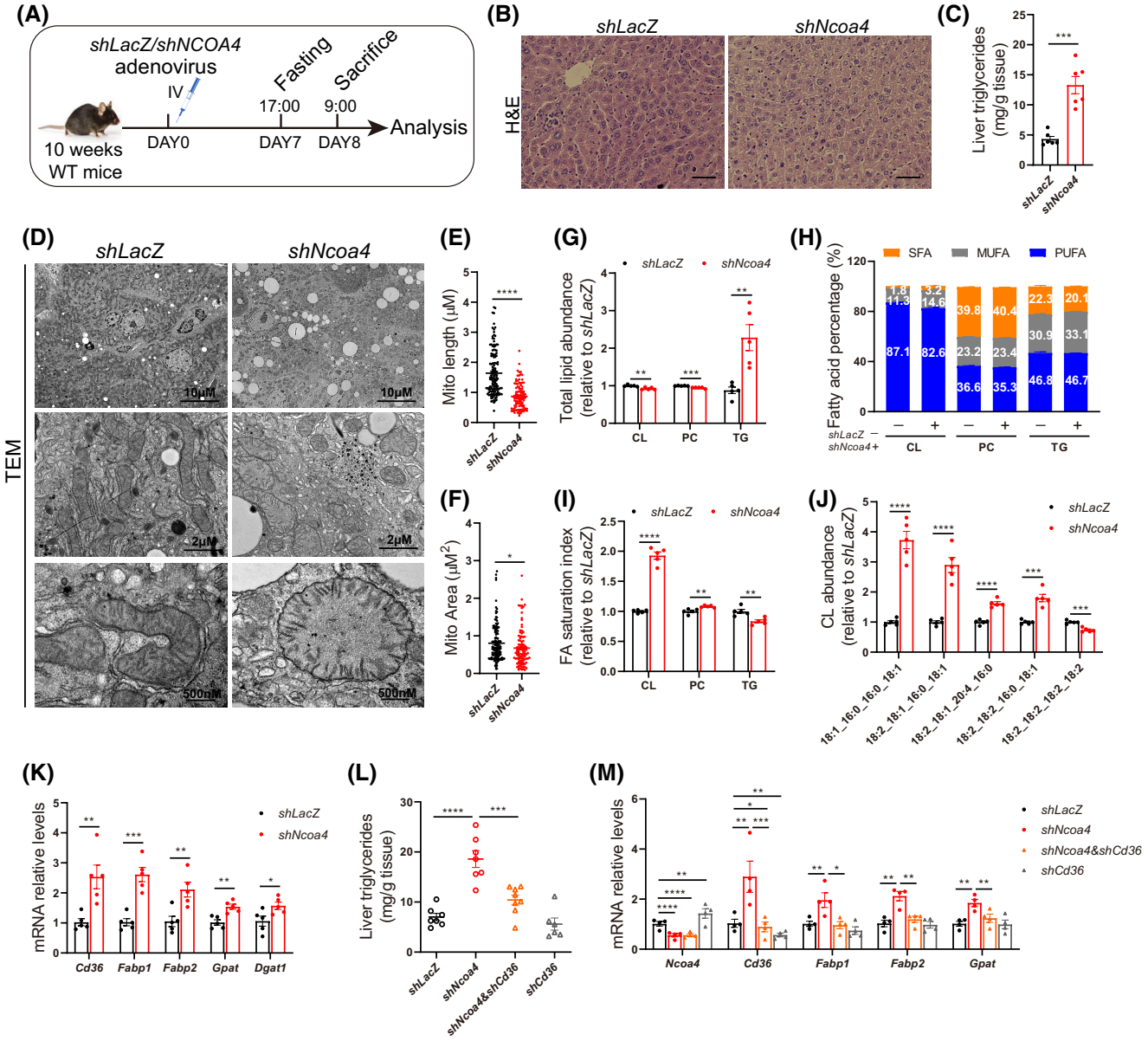

FIGURE 6 Ferritinophagy is not required for hepatic re-esterification of fatty acids under fasting conditions. (A) Schematic illustration of experimental design. Ten-week-old C57BL/6J male mice were tail vein–injected with adenovirus-expressing *shLacZ* or *shNcoa4*. Mice were sacrificed 8 days following adenovirus administration after overnight fasting (5:00 p.m.–9:00 a.m.). (B,C) H&E staining (B) and triglyceride measurements (C) of the liver tissues of *shLacZ* and *shNcoa4* fasted mice (n = 5–6 mice/group). Scale bar, 50 μm. (D–F) Transmission electron microscopy (TEM) analysis of hepatic mitochondrial morphology (D) from mice expressing *shLacZ* or *shNcoa4* after overnight fasting; over 100 mitochondria in each group were quantified for average mitochondrial length (E) and area (F). (G–J) Mass spectrometry quantification of the relative abundance of total CL, PC, and TG (G), the fatty acid compositions of CL, PC, and TG (H), calculated indices of fatty acid saturation (C16:0/C18:1) for CL, PC, and TG (I), and the measured C16:0-containing or C18:2-only CLs (J) in the liver tissues of *Ncoa4*-deficient, fasted mice (n = 5 mice/group). (K) Real-time PCR measurements of hepatic *Cd36*, fatty acid–binding proteins (*Fabps*), glycerol-3-phosphate acyltransferase (*Gpat*), and diacylglycerol O-acyltransferase 1 (*Dgat1*) transcript levels from mice treated as in (A) (n = 4 mice/group). (L) Measurements of liver triglyceride levels from mice expressing *shLacZ*, *shNcoa4*, *shCd36*, or double *shLacZ and shCd36*. Mice were sacrificed 8 days following adenovirus administration after overnight fasting (5:00 p.m.–9:00 a.m.) as in (A) (n = 6–8 mice/group). (M) Real-time PCR measurements of hepatic *Ncoa4*, *Cd36*, *Fabps*, and *Gpat* transcript levels from mice treated as in (L) (n = 4 mice/group). Data are presented as mean ± SEM; **p* < 0.05, ***p* < 0.01, ****p* < 0.001, *****p* < 0.0001; Student's *t* test (see also Figure S5).

dietary unsaturated fatty acid content may modify the relationship between ferritinophagy and hepatic steatosis/obesity. When the dietary fatty acid content is low, the body will be more dependent on ferritinophagy to desaturate fatty acids for triglyceride synthesis. However, under circumstances of ample dietary unsaturated fatty acids, high ferritinophagy activity may improve mitochondrial function through enhanced cardiolipin synthesis to reduce obesity and hepatic steatosis. Therefore, monitoring ferritinophagy status

and dietary/plasma fatty acid composition may be important to dissect the relationship between iron and DIOS. Although it is challenging to measure ferritinophagy in clinical samples, the circulating ferritin secreted from the lysosome[43] may serve as a surrogate marker. There are early indications that hepatic *NCOA4* expression correlates with serum ferritin levels: obese patients with diabetes have higher levels of serum ferritin levels than patients without diabetes,[44] and they often present higher hepatic *NCOA4* expression.[45] Future research is needed to establish their quantitative correlation.

Initially, we were concerned about the possibility of *Ncoa4* deficiency in exacerbating lipotoxicity in obese mice. Feedback inhibition of lipogenesis may play a role in ameliorating liver damage in the *shNcoa4* obese mice. Alternatively, ferritinophagy is an essential component of ferroptosis and many diseases.[33,46–48] We may speculate that the manifestation of metabolic syndrome requires ferritinophagy-derived iron to generate oxidative stress and inflammation. Along this line, transcriptome analysis from clinical samples does show that obese patients without diabetes have a lower hepatic expression of *NCOA4* compared with lean individuals or obese patients with diabetes, and *NCOA4* expression is positively associated with gluconeogenic and lipogenic gene expression in obese patients.[45] Therefore, chemical inhibition of ferritinophagy may be a viable approach to tackle NAFLD and NASH. The lack of effect of hepatic *Ncoa4* deficiency on erythropoiesis reported herein and elsewhere[49] suggests a good safety profile in this approach. Nevertheless, dietary fatty acid composition, CD36 induction, and compensatory up-regulation in iron absorption may all affect the long-term utility of such a strategy.

ACKNOWLEDGMENT

The authors thank Xiaohui Liu, Lina Xu, Yupei Jiao, Xueying Wang, and Yusong Wang from the Metabolomics Facility at Technology Center for Protein Sciences at Tsinghua University for the lipidomic analysis; Zai Chang from Tsinghua Model Animal Center for the mouse husbandry and metabolic phenotyping; Cyagen (Suzhou, China) for generating the *Ncoa4*$^{flox/flox}$ mice; Drs. Xiaowei Chen, Wade Harper, Peng Li, Joseph Mancias, Fudi Wang, Montana Vanity, Kuanyu Li, and Qiaoran Xi for sharing equipment, reagents, and mouse lines; and Fudi Wang and Junxia Min for their careful reading of this manuscript.

FUNDING INFORMATION

Supported by the National Key Research and Development Program of China (2017YFA0504603 and 2016YFA0502002), National Natural Science Foundation of China (NSFC 31671229 and 81,471,072), the Tsinghua-Peking Center for Life Sciences, and Guangzhou Laboratory to S.F.

CONFLICT OF INTEREST

Nothing to report.

REFERENCES

1. Andrews NC, Schmidt PJ. Iron homeostasis. Annu Rev Physiol. 2007;69:69–85.
2. Zhang C. Essential functions of iron-requiring proteins in DNA replication, repair and cell cycle control. Protein Cell. 2014;5:750–60.
3. Winterbourn CC. Toxicity of iron and hydrogen peroxide: the Fenton reaction. Toxicol Lett. 1995;82–83:969–74.
4. Pantopoulos K, Porwal SK, Tartakoff A, Devireddy L. Mechanisms of mammalian iron homeostasis. Biochemistry. 2012;51:5705–24.
5. Britton LJ, Subramaniam VN, Crawford DH. Iron and non-alcoholic fatty liver disease. World J Gastroenterol. 2016;22:8112–22.
6. Datz C, Felder TK, Niederseer D, Aigner E. Iron homeostasis in the metabolic syndrome. Eur J Clin Invest. 2013;43:215–24.
7. Rolo AP, Teodoro JS, Palmeira CM. Role of oxidative stress in the pathogenesis of nonalcoholic steatohepatitis. Free Radic Biol Med. 2012;52:59–69.
8. Andreo U, Elkind J, Blachford C, Cederbaum AI, Fisher EA. Role of superoxide radical anion in the mechanism of apoB100 degradation induced by DHA in hepatic cells. FASEB J. 2011;25:3554–60.
9. Pan M, Cederbaum AI, Zhang YL, Ginsberg HN, Williams KJ, Fisher EA. Lipid peroxidation and oxidant stress regulate hepatic apolipoprotein B degradation and VLDL production. J Clin Invest. 2004;113:1277–87.
10. George DK, Goldwurm S, MacDonald GA, Cowley LL, Walker NI, Ward PJ, et al. Increased hepatic iron concentration in nonalcoholic steatohepatitis is associated with increased fibrosis. Gastroenterology. 1998;114:311–8.
11. Handa P, Morgan-Stevenson V, Maliken BD, Nelson JE, Washington S, Westerman M, et al. Iron overload results in hepatic oxidative stress, immune cell activation, and hepatocellular ballooning injury, leading to nonalcoholic steatohepatitis in genetically obese mice. Am J Physiol Gastrointest Liver Physiol. 2016;310:G117–27.
12. Graham RM, Chua AC, Carter KW, Delima RD, Johnstone D, Herbison CE, et al. Hepatic iron loading in mice increases cholesterol biosynthesis. Hepatology. 2010;52:462–71.
13. James JV, Varghese J, McKie AT, Vaulont S, Jacob M. Enhanced insulin signaling and its downstream effects in iron-overloaded primary hepatocytes from hepcidin knock-out mice. Biochim Biophys Acta Mol Cell Res. 2020;1867:118621.
14. Tan TC, Crawford DH, Jaskowski LA, Subramaniam VN, Clouston AD, Crane DI, et al. Excess iron modulates endoplasmic reticulum stress-associated pathways in a mouse model of alcohol and high-fat diet-induced liver injury. Lab Invest. 2013;93:1295–312.
15. Moris W, Verhaegh P, Jonkers D, Deursen CV, Koek G. Hyperferritinemia in nonalcoholic fatty liver disease: iron accumulation or inflammation? Semin Liver Dis. 2019;39:476–82.
16. Nead KG, Halterman JS, Kaczorowski JM, Auinger P, Weitzman M. Overweight children and adolescents: a risk group for iron deficiency. Pediatrics. 2004;114:104–8.
17. Cheng HL, Bryant C, Cook R, O'Connor H, Rooney K, Steinbeck K. The relationship between obesity and hypoferraemia in adults: a systematic review. Obes Rev. 2012;13:150–61.
18. Sal E, Yenicesu I, Celik N, Pasaoglu H, Celik B, Pasaoglu OT, et al. Relationship between obesity and iron deficiency anemia: is there a role of hepcidin? Hematology. 2018;23:542–8.
19. Cepeda-Lopez AC, Zimmermann MB, Wussler S, Melse-Boonstra A, Naef N, Mueller SM, et al. Greater blood volume and Hb mass in obese women quantified by the

carbon monoxide-rebreathing method affects interpretation of iron biomarkers and iron requirements. Int J Obes (Lond). 2019;43:999–1008.
20. Aeberli I, Hurrell RF, Zimmermann MB. Overweight children have higher circulating hepcidin concentrations and lower iron status but have dietary iron intakes and bioavailability comparable with normal weight children. Int J Obes (Lond). 2009;33:1111–7.
21. Amato A, Santoro N, Calabrò P, Grandone A, Swinkels DW, Perrone L, et al. Effect of body mass index reduction on serum hepcidin levels and iron status in obese children. Int J Obes (Lond). 2010;34:1772–4.
22. Aigner E, Feldman A, Datz C. Obesity as an emerging risk factor for iron deficiency. Nutrients. 2014;6:3587–600.
23. Gartner A, Berger J, Bour A, El Ati J, Traissac P, Landais E, et al. Assessment of iron deficiency in the context of the obesity epidemic: importance of correcting serum ferritin concentrations for inflammation. Am J Clin Nutr. 2013;98:821–6.
24. Rametta R, Fracanzani AL, Fargion S, Dongiovanni P. Dysmetabolic hyperferritinemia and dysmetabolic iron overload syndrome (DIOS): two related conditions or different entities? Curr Pharm Des. 2020;26:1025–35.
25. Arosio P, Elia L, Poli M. Ferritin, cellular iron storage and regulation. IUBMB Life. 2017;69:414–22.
26. Kidane TZ, Sauble E, Linder MC. Release of iron from ferritin requires lysosomal activity. Am J Physiol Cell Physiol. 2006;291:C445–55.
27. Zhang Y, Mikhael M, Xu D, Li Y, Soe-Lin S, Ning B, et al. Lysosomal proteolysis is the primary degradation pathway for cytosolic ferritin and cytosolic ferritin degradation is necessary for iron exit. Antioxid Redox Signal. 2010;13:999–1009.
28. Dowdle WE, Nyfeler B, Nagel J, Elling RA, Liu S, Triantafellow E, et al. Selective VPS34 inhibitor blocks autophagy and uncovers a role for NCOA4 in ferritin degradation and iron homeostasis in vivo. Nat Cell Biol. 2014;16:1069–79.
29. Mancias JD, Wang X, Gygi SP, Harper JW, Kimmelman AC. Quantitative proteomics identifies NCOA4 as the cargo receptor mediating ferritinophagy. Nature. 2014;509:105–9.
30. Fujimaki M, Furuya N, Saiki S, Amo T, Imamichi Y, Hattori N. Iron supply via NCOA4-mediated ferritin degradation maintains mitochondrial functions. Mol Cell Biol. 2019;39:e00010-19.
31. Mancias JD, Pontano Vaites L, Nissim S, Biancur DE, Kim AJ, Wang X, et al. Ferritinophagy via NCOA4 is required for erythropoiesis and is regulated by iron dependent HERC2-mediated proteolysis. Elife. 2015;4:e10308.
32. Santana-Codina N, Gableske S, Quiles del Rey M, Malachowska B, Jedrychowski MP, Biancur DE, et al. NCOA4 maintains murine erythropoiesis via cell autonomous and non-autonomous mechanisms. Haematologica. 2019;104:1342–54.
33. Sui S, Zhang J, Xu S, Wang Q, Wang P, Pang D. Ferritinophagy is required for the induction of ferroptosis by the bromodomain protein BRD4 inhibitor (+)-JQ1 in cancer cells. Cell Death Dis. 2019;10:331.
34. Anderson ER, Shah YM. Iron homeostasis in the liver. Compr Physiol. 2013;3:315–30.
35. Wang H, Klein MG, Zou H, Lane W, Snell G, Levin I. 331 crystal structure of human stearoyl-coenzyme A desaturase in complex with substrate. Nat Struct Mol Biol. 2015;22:581–5.
36. Bai Y, McCoy JG, Levin EJ, Sobrado P, Rajashankar KR, Fox BG, et al. X-ray structure of a mammalian stearoyl-CoA desaturase. Nature. 2015;524:252–6.
37. Fu S, Yang L, Li P, Hofmann O, Dicker L, Hide W, et al. Aberrant lipid metabolism disrupts calcium homeostasis causing liver endoplasmic reticulum stress in obesity. Nature. 2011;473:528–31.
38. Listenberger LL, Han X, Lewis SE, Cases S, Farese RV Jr, Ory DS, et al. Triglyceride accumulation protects against fatty acid-induced lipotoxicity. Proc Natl Acad Sci U S A. 2003;100:3077–82.
39. Jung IR, Choi SE, Jung JG, Lee SA, Han SJ, Kim HJ, et al. Involvement of iron depletion in palmitate-induced lipotoxicity of beta cells. Mol Cell Endocrinol. 2015;407:74–84.
40. Vecchi C, Montosi G, Garuti C, Corradini E, Sabelli M, Canali S, et al. Gluconeogenic signals regulate iron homeostasis via hepcidin in mice. Gastroenterology. 2014;146:1060–9.
41. Wang X, Fang X, Wang F. Pleiotropic actions of iron balance in diabetes mellitus. Rev Endocr Metab Disord. 2015;16:15–23.
42. Gonzalez-Dominguez A, Visiedo-Garcia FM, Dominguez-Riscart J, Gonzalez-Dominguez R, Mateos RM, Lechuga-Sancho AM. Iron metabolism in obesity and metabolic syndrome. Int J Mol Sci. 2020;21:5529.
43. Truman-Rosentsvit M, Berenbaum D, Spektor L, Cohen LA, Belizowsky-Moshe S, Lifshitz L, et al. Ferritin is secreted via 2 distinct nonclassical vesicular pathways. Blood. 2018;131:342–52.
44. Lecube A, Hernández C, Pelegrí D, Simó R. Factors accounting for high ferritin levels in obesity. Int J Obes (Lond). 2008;32:1665–9.
45. Pihlajamäki J, Boes T, Kim EY, Dearie F, Kim BW, Schroeder J, et al. Thyroid hormone-related regulation of gene expression in human fatty liver. J Clin Endocrinol Metab. 2009;94:3521–9.
46. Hou W, Xie Y, Song X, Sun X, Lotze MT, Zeh HJ 3rd, et al. Autophagy promotes ferroptosis by degradation of ferritin. Autophagy. 2016;12:1425–8.
47. Santana-Codina N, Mancias JD. The role of NCOA4-mediated ferritinophagy in health and disease. Pharmaceuticals (Basel). 2018;11:114.
48. Fang X, Wang H, Han D, Xie E, Yang X, Wei J, et al. Ferroptosis as a target for protection against cardiomyopathy. Proc Natl Acad Sci U S A. 2019;116:2672–80.
49. Li X, Lozovatsky L, Sukumaran A, Gonzalez L, Jain A, Liu D, et al. NCOA4 is regulated by HIF and mediates mobilization of murine hepatic iron stores after blood loss. Blood. 2020;136:2691–702.

SUPPORTING INFORMATION

Additional supporting information can be found online in the Supporting Information section at the end of this article.

How to cite this article: Li N, Liao Y, Huang H, Fu S. Co-regulation of hepatic steatosis by ferritinophagy and unsaturated fatty acid supply. Hepatol Commun. 2022;6:2640–2653. https://doi.org/10.1002/hep4.2040